Rare Hadronic B Decays to Vector, Axial-Vector and Tensors

Y.Y. Gao (on behalf of the *BABAR*Collaboration) [a]

[a]2575 Sand Hill Road, Menlo Park, CA, 94025, USA

We review the recent *BABAR* measurements of several rare B decays, including vector–axial-vector decays $B^\pm \to \varphi K_1(1270)^\pm$, $B^\pm \to \varphi K_1(1400)^\pm$ and $B^\pm \to b_1^\mp \rho^\pm$, vector-vector decays $B^\pm \to \varphi K^*(1410)^\pm$, $B^0 \to K^{*0}\bar{K}^{*0}$, $B^0 \to K^{*0}K^{*0}$ and $B^0 \to K^{*+}K^{*-}$, vector-tensor decays $B^\pm \to \varphi K_2^*(1430)^\pm$ and $\varphi K_2(1770)/(1820)^\pm$, and vector-scalar decays $B^\pm \to \varphi K_0^*(1430)^\pm$. Understanding the observed polarization pattern requires amplitude contributions from an uncertain source.

1. Introduction

Measurements of polarization in rare vector-vector B meson decay, such as $B \to \varphi K^*$ [1,2], have revealed an unexpectedly large fraction of transverse polarization and suggested contributions to the decay amplitude which were previously neglected. In the standard model (SM), the decays are dominated by the $b \to s$ QCD penguin loop, shown in Fig. 1 (a). Decays to other excited spin-J kaons $K_J^{(*)}$ can also take place. The differential width for a $B \to \varphi K_J^{(*)}$ decay has three complex amplitudes $A_{J\lambda}$, which describe the three helicity states $\lambda = 0, \pm 1$, except when $J = 0$. The hierarchy of the $A_{J\lambda}$ amplitudes is sensitive to the $(V - A)$ structure of the weak interactions, helicity conservation in strong interactions, and the s-quark spin flip suppression in the penguin decay [3–5], and therefore is sensitive to physics beyond the SM.

However, all previous studies have been limited to the two-body $K_J^* \to K\pi$ decays, thus considering only the spin-parity K_J^* states with $P = (-1)^J$. In this talk, we report on first time measurements with the three-body final states $K_J^{(*)} \to K\pi\pi$ which include $P = (-1)^{J+1}$ mesons such as axial-vectors $K_1(1270)$ and $K_1(1400)$, vector $K^*(1410)$, tensors $K_2(1770)$ and $K_2(1820)$ [6]. We complement these measurements with the two-body $K_J^{(*)}$ final states in the $B^\pm$ decays to final states with φ and $K_0^*(1430)^\pm$ and $K_2^*(1430)^\pm$, to be compared with earlier measurements on the corresponding B^0 decays [1].

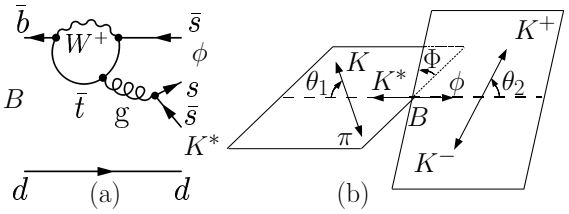

Figure 1. (a) Feynman diagram describing the $B^0 \to \varphi K^{*0}$ decay; (b) definition of decay angles given in the rest frames of the decaying parents.

On the other hand, decays proceeding via electro-weak and gluonic $b \to d$ penguin diagrams have only been measured in the decays $B \to \rho\gamma$ [7] and $B \to K^0\bar{K}^0$ [8]. The same $b \to d$ transition can also be measured in charmless decays $B^0 \to K^{*0}\bar{K}^{*0}$, with upper limits of branching fractions placed experimentally. The theoretical calculated branching fractions cover the range $(0.16\text{-}0.96) \times 10^{-6}$. With enough statistics, the potential polarization measurement can also provide insight to the polarization puzzle. The SM suppressed decay $B^0 \to K^{*0}K^{*0}$ could appear via an intermediate heavy boson, while decay $B^0 \to K^{*+}K^{*-}$ is expected to occur through a $b \to u$ transition via W-exchange, or from final-state interactions.

In this talk, we also report on vector–axial-vector (VA) decays $B^0 \to b_1^\mp \rho^\pm$, motivated by

Cheng and Yang's recent calculations[9] on VA decays focusing on the penguin annihilation amplitudes. These decays have a similar helicity structure as the $B \to \varphi K_J^{(*)}$ decays. The branching fraction of the decay $B^0 \to b_1^- \rho^+$ is expected to be much larger than the decay $B^0 \to b_1^+ \rho^-$ due to the second-class current rule. We report the sum of the two. The b_1 meson is reconstructed through its dominant decay to an $\omega\pi$ state, while the ρ decays to $\pi^\pm\pi^0$.

2. Analysis Technique Overview

We use data collected with the *BABAR* detector [12] at the PEP-II e^+e^- collider. A sample of (465 ± 5) million $\Upsilon(4S) \to B\overline{B}$ events was recorded at the the e^+e^- center-of-mass energy $\sqrt{s} = 10.58\,\mathrm{GeV}$. In this talk, we focus on the analysis description of $B \to \varphi K_J^{(*)}$, while details for the other modes are given in reference [10,11]. Momenta of charged particles are measured in a tracking system consisting of a silicon vertex tracker with five double-sided layers and a 40-layer drift chamber, both within the 1.5-T magnetic field of a solenoid. Identification of charged particles is provided by measurements of the energy loss in the tracking devices and by a ring-imaging Cherenkov detector. Photons are detected by a CsI(Tl) electromagnetic calorimeter. We search for $B^\pm \to \varphi K_J^{(*)\pm}$ decays using three final states of the $K_J^{(*)\pm}$ decay: $K_S^0\pi^\pm$, $K^\pm\pi^0$, and $K^\pm\pi^+\pi^-$, where $K_S^0 \to \pi^+\pi^-$ and $\pi^0 \to \gamma\gamma$. The two helicity angles θ_i are defined as the angle between the direction of the K or K^+ meson from $K^* \to K\pi$ (θ_1) or $\varphi \to K^+K^-$ (θ_2) and the direction opposite to the B in the K^* or φ rest frame, shown in Fig. 1 (b). For $K_J^{(*)\pm} \to K\pi\pi$ modes, the normal to the three-body decay plane for $K_J^{(*)} \to K\pi\pi$ is chosen as the analyzer of the $K_J^{(*)}$ polarization instead. We define $\mathcal{H}_i = \cos\theta_i$.

We identify B meson candidates using two kinematic variables: $m_{\rm ES} = (s/4 - \mathbf{p}_B^2)^{1/2}$ and $\Delta E = \sqrt{s}/2 - E_B$, where $(E_B, \mathbf{p}_B)$ is the four-momentum of the B candidate in the e^+e^- center-of-mass frame. We require $m_{\rm ES} > 5.25$ GeV and $|\Delta E| < 0.1$ (or 0.08 for $K_J^{(*)\pm} \to K^\pm\pi^+\pi^-$) GeV. We also cut on the invariant masses to satisfy $1.1 < m_{K\pi} < 1.6$ GeV $1.1 < m_{K\pi\pi} < 2.1$ GeV, and $0.99 < m_{K^+K^-} < 1.05$ GeV. The dominant background comes from $e^+e^- \to$ light quark we use the angle θ_T between the thrust axis of the B-candidate decay products and that of the rest of the event requiring $|\cos\theta_T| < 0.8$, and a Fisher discriminant $\mathcal{F}$ which combines event-shape parameters [13]. To reduce combinatorial background in the mode $K_J^{(*)\pm} \to K^\pm\pi^0$, we require $\mathcal{H}_1 < 0.6$. When more than one candidate is reconstructed (7.6% of events with $K_S^0\pi^\pm$, 2.9% with $K^\pm\pi^0$, and 14.6% with $K^\pm\pi^+\pi^-$), we select the one whose χ^2 of the charged-track vertex fit combined with χ^2 of the invariant mass consistency of the K_S^0 or π^0 candidate, is the lowest.

We use an unbinned extended maximum-likelihood fit [1] to extract the event yields n_j and the probability density function (PDF) parameters, denoted by $\boldsymbol{\zeta}$ and $\boldsymbol{\xi}$, to be described below. The index j represents the event categories, which include the signal modes, continuum background and several resonant and non-resonant B-decay background modes. In the $B^\pm \to \varphi K_J^{*\pm} \to (K^+K^-)(K\pi)$ topology, the following event categories are considered: $\varphi K_2^*(1430)^\pm$, $\varphi(K\pi)_0^{*\pm}$, and $f_0(K\pi)_0^{*\pm}$, where the $J^P = 0^+$ $(K\pi)_0^{*\pm}$ contribution includes both a nonresonant component and the $K_0^*(1430)^\pm$ resonance [17]. In the $B^\pm \to \varphi K_J^{(*)\pm} \to (K^+K^-)(K\pi\pi)$ topology, we consider $\varphi K_1(1270)^\pm$, $\varphi K_1(1400)^\pm$, $\varphi K_2^*(1430)^\pm$, $\varphi K^*(1410)^\pm$, $\varphi K_2(1820)^\pm$, a nonresonant $\varphi K^\pm\pi^+\pi^-$, and $f_0 K_1(1400)^\pm$ contributions. In the $B^\pm \to \varphi K_J^{(*)\pm} \to (K^+K^-)(K\pi\pi)$, the mode $\varphi K_2(1770)^\pm$ is also considered in place of $\varphi K_2(1820)^\pm$. In all cases, the modes with f_0 model can account for a possible broad non-φ (K^+K^-) contributions under the φ.

The extended likelihood is $\mathcal{L} = \exp(-\sum n_j) \prod \mathcal{L}_i$. The likelihood $\mathcal{L}_i$ for candidate i is defined as $\mathcal{L}_i = \sum_{j,k} n_j^k \mathcal{P}_j^k(\mathbf{x_i};\, \boldsymbol{\zeta},\, \boldsymbol{\xi})$, where $\mathcal{P}_j^k$ is the PDF for variables We use variables $\mathbf{x_i} = \{\mathcal{H}_1,\ \mathcal{H}_2,\ m_{K\pi(\pi)},\ m_{K^+K^-},\ \Delta E,\ m_{\rm ES},\ \mathcal{F},\ Q\}$. The flavor index k corresponds to the b-quark flavor sign Q, being opposite to the charge of the B meson candidate. That makes $\mathcal{P}_j^k \equiv \mathcal{P}_j \times \delta_{kQ}$. The $\boldsymbol{\zeta}$ are the polarization pa-

rameters, only relevant for the signal PDF. The $\boldsymbol{\xi}$ parameters describe the background or the remaining signal PDFs, which are left free to vary in the fit for the combinatorial background and are fixed to the values extracted from Monte Carlo (MC) simulation [14] and calibration $B \to \overline{D}\pi$ decays in other cases.

The signal PDF for a given candidate i is a joint PDF for the helicity angles and resonance mass, and the product of the PDFs for each of the remaining variables. The helicity part of the signal PDF is the ideal angular distribution [15] multiplied by an empirical acceptance function $\mathcal{G}(\mathcal{H}_1, \mathcal{H}_2)$. A relativistic spin-$J$ Breit–Wigner amplitude parameterization is used for the resonance masses [5,16], and the $J^P = 0^+$ $(K\pi)_0^{*\pm}$ $m_{K\pi}$ amplitude is parameterized with the LASS function [17]. The nonresonant $\varphi K^\pm\pi^+\pi^-$ contribution is modeled through $K^*(892)\pi \to K\pi\pi$ decay. We use a sum of Gaussian functions for the parameterization of ΔE, $m_{\rm ES}$, and $\mathcal{F}$.

The interference between the $J = 2$ and 0 $(K\pi)^\pm$ contributions is modeled with the term $2\mathcal{R}\mathrm{e}(A_{20}A_{00}^*)$, with the three-dimensional angular and $m_{K\pi}$ parameterization. We allow an unconstrained flavor-dependent overall shift $(\delta_0 + \Delta\delta_0 \times Q)$ between the LASS amplitude phase and the tensor resonance amplitude phase. The polarization parameters $\boldsymbol{\zeta}$ include the fractions of longitudinal polarization $f_L = |A_{J0}|^2/\Sigma|A_{J\lambda}|^2$ in several channels, δ_0, and $\Delta\delta_0$. Similar interference between the $K_1(1270)^\pm$ and $K_1(1400)^\pm$ contributions is allowed in the study of systematic uncertainties but is not included in the nominal fit due to observed dominance of only one mode and therefore unconstrained phase of the interference.

Since the $K_2^*(1430)^\pm$ meson contributes to all three $K^0\pi^\pm$, $K^\pm\pi^0$, and $K^\pm\pi^+\pi^-$ final states and $(K\pi)_0^{*\pm}$ contributes to two $K\pi$ final states in this analysis, we consider the total $\mathcal{L}$ as a product of three likelihoods constructed for each of the three channels. The corresponding yields in different channels are related by the relative efficiency. We fit the yields in each charge category k independently and report them in the form of the total yield $n_j = n_j^+ + n_j^-$ and direct-*CP* asymmetry $\mathcal{A}_{CP} = (n_j^+ - n_j^-)/n_j$. The combinatorial background PDF is the product of the PDFs for independent variables and is found to describe well both the dominant quark-antiquark background and the background from random combinations of B tracks. We use polynomials for the PDFs, except for $m_{\rm ES}$ and $\mathcal{F}$ distributions which are parameterized by an empirical phase-space function and by Gaussian functions, respectively. Resonance production occurs in the background and is taken into account in the PDF.

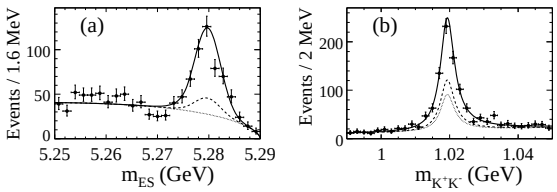

Figure 2. Projections onto the variables $m_{\rm ES}$ (a), and $m_{K\overline{K}}$ (b) for the signal $B^+ \to \varphi(K\pi)$ and $B^+ \to \varphi(K\pi\pi)$ candidates. Data distributions are shown with a requirement on the signal-to-background probability ratio calculated with the plotted variable excluded. The solid (dotted) lines show the signal-plus-background (combinatorial background) PDF projections, while the dashed lines show the full PDF projections excluding the signal.

3. Results

We observe decays $B^\pm \to \varphi K_1(1270)^\pm$ and $B^0 \to K^{*0}\bar{K}^{*0}$, with branching fractions of $6.1 \pm 1.6 \pm 1.1 \times 10^{-6}$ and $1.28^{+0.35}_{-0.30} \pm 0.11 \times 10^{-6}$, and significance of 5.0σ and 6.0σ respectively. The significance is defined as the square root of the change in $2\ln\mathcal{L}$ when the yield is constrained to zero in the likelihood $\mathcal{L}$. The f_L of the vector–axial-vector decays $B^\pm \to \varphi K_1^\pm$ is measured as $0.46^{+0.12\ +0.03}_{-0.13\ -0.17}$, in sharp contrast to the SM predicated longitudinal dominance. The polarization of the vector-vector decay $B^0 \to K^{*0}\bar{K}^{*0}$ is measured as $0.80^{+0.10}_{-0.12} \pm 0.06$, consistent with the SM predication. However, as indicated earlier, decays $B \to \phi K_J^{(*)}$ and $B \to K^{*0}\bar{K}^{*0}$ proceed through

similar penguin loop, with the former via $b \to s$ transition, and the latter via $b \to d$ transition. Thus the f_L difference between these two vector-vector decays may help resolve the polarization puzzle.

We measure the branching fractions of vector-scalar decays $\mathcal{B}(B^\pm \to \varphi(K\pi)_0^{*\pm}) = 8.3 \pm 1.4 \pm 0.8 \times 10^{-6}$ and vector-tensor decays $\mathcal{B}(B^\pm \to \varphi K_2^{*\pm}) = 8.4 \pm 1.8 \pm 0.9 \times 10^{-6}$ with significance of 8.2σ and 5.5σ respectively. We extract the branching fraction of the resonant decays $B^\pm \to \varphi K_0^{*\pm}$ as $7.0 \pm 1.3 \pm 0.9 \times 10^{-6}$, from the coherent sum of resonant and nonresonant $J^P = 0^+$ mode $B^\pm \to \varphi(K\pi)_0^{*\pm}$. The f_L of vector-tensor decays $B^\pm \to \varphi K_2^{*\pm}$ is measured as $0.80^{+0.09}_{-0.10} \pm 0.03$, consistent with the SM prediction. However, its difference from the f_L measured in the vector-vector and vector–axial-vector decays adds additional flavor to the existing polarization puzzle.

Tight upper limits on the branching fractions at 90% confidence level are placed for the other decay modes, with significance $< 2\sigma$. We measure the branching fractions in the unit of 10^{-6}:

- $\mathcal{B}(B^\pm \to \varphi K_1^\pm(1400)) < 3.2 (0.3 \pm 1.6 \pm 0.7)$
- $\mathcal{B}(B^\pm \to \varphi K^{*\pm}(1410)) < 4.8 (2.4 \pm 1.2^{+0.8}_{-1.2})$
- $\mathcal{B}(B^\pm \to \varphi K_2^\pm(1770)) < 15.0$
- $\mathcal{B}(B^\pm \to \varphi K_2^\pm(1820)) < 16.3$
- $\mathcal{B}(B^0 \to K^{*0} K^{*0} < 0.41 (0.11^{+0.16}_{-0.11} \pm 0.04)$
- $\mathcal{B}(B^0 \to K^{*+} K^{*-} < 2.0$
- $\mathcal{B}(B^0 \to b_1^\mp \rho^\pm) < 1.7 (-0.1 \pm 0.9 \pm 0.7)$.

The numbers in the parenthesis represent the center values. In the branching fraction calculations we assume $K_2 \to K_2^*(1430)\pi$ and $\mathcal{B}(K^*(1410) \to K^*\pi) = 0.934 \pm 0.013$ [5].

The signal of $B^\pm$ decays is illustrated in the projection plots in Figs. 2 and 3, where in the latter we enhance either the $\varphi K_1(1270)^\pm$ signal (left) or the $\varphi K_2^*(1430)^\pm$ signal (right). All the flavor asymmetry $\mathcal{A}_{CP}$ measurements are consistent with 0. Comprehensive systematic studies are performed in all the analysis, please see the details at the papers [6,10,11].

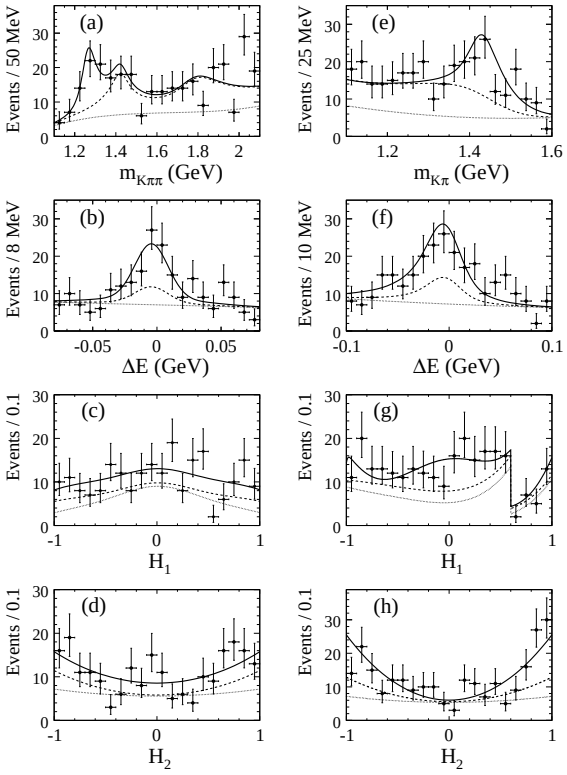

Figure 3. Left column: projections onto the variables $m_{K\pi\pi}$ (a), ΔE (b), $\mathcal{H}_1$ (c), and $\mathcal{H}_2$ (d) for the signal $\varphi K_1(1270)^\pm$ candidate. Right column: projections onto the variables $m_{K\pi}$ (e), ΔE (f), $\mathcal{H}_1$ (g), and $\mathcal{H}_2$ (h) for the signal $\varphi K_2^*(1430)^\pm$ and $\varphi(K\pi)_0^{*\pm}$ candidates combined. The step in (g) is due to selection requirement $\mathcal{H}_1 < 0.6$ in the channel with π^0. Data distributions are shown with a requirement on the signal-to-background probability ratio calculated with the plotted variable excluded. The solid (dotted) lines show the signal-plus-background (combinatorial background) PDF projections, while the dashed lines show the full PDF projections excluding $\varphi K_1^\pm$ (left) or $\varphi K_2^*(1430)^\pm$ (right).

4. Summary

In summary, we have discussed amplitude analysis of various rare charmless B decays, focusing on the decays $B^{\pm} \to \varphi K_J^{(*\pm)}$. Observations are made for decays $B^{\pm} \to \varphi K_1(1270)^{\pm}$ and $B^0 \to K^{*0}\bar{K}^{*0}$. The polarization measurements in the vector-tensor $B \to \varphi K_2^*$ decay and vector-vector decay $B \to K^*\bar{K}^*$ are consistent and with the SM expectation of the longitudinal polarization dominance. However, our first measurement of polarization in a vector–axial-vector B meson decay indicates a large fraction of transverse amplitude, similar to polarization observed in the vector-vector final state $B \to \varphi K^*(892)$ [1,2]. Both measurements indicate substantial A_{1+1} (or still possible A_{1-1} for vector–axial-vector decay) amplitude from an uncertain source [3] and may indicate new amplitude contributions.

REFERENCES

1. *BABAR* Collaboration, B. Aubert *et al.*, Phys. Rev. Lett. **91**, 171802 (2003); Phys. Rev. Lett. **93**, 231804 (2004). Phys. Rev. Lett. **98**, 051801 (2007); Phys. Rev. Lett. **99**, 201802 (2007); Phys. Rev. D **76**, 051103 (2007).
2. Belle Collaboration, K.-F. Chen *et al.*, Phys. Rev. Lett. **91**, 201801 (2003); Phys. Rev. Lett. **94**, 221804 (2005).
3. A. L. Kagan, Phys. Lett. B **601**, 151 (2004); H.-n. Li and S. Mishima, Phys. Rev. D **71**, 054025 (2005); C.-H. Chen et al., Phys. Rev. D **72**, 054011 (2005); M. Beneke *et al.*, Nucl. Phys. B **774**, 64 (2007); C.-H. Chen and C.-Q. Geng, Phys. Rev. D **75**, 054010 (2007); A. Datta *et al.*, Phys. Rev. D **76**, 034015 (2007); H.-Y. Cheng, K.-C. Yang, arXiv:0805.0329 [hep-ph].
4. A. Gritsan and J. G. Smith, "Polarization in B Decays" review in [5], J. Phys. G33, 833 (2006).
5. Particle Data Group, W.-M. Yao *et al.*, J. Phys. G33, 1 (2006).
6. *BABAR* Collaboration, B. Aubert *et al.*, arXiv:0806.4416 [hep-ex]
7. B. Aubert *et al.* (*BABAR* Collaboration), Phys. Rev. Lett. **98**, 151802 (2007); D. Mohapatra *et al.* (Belle Collaboration), Phys. Rev. Lett.**96**, 221601 (2006).
8. B. Aubert *et al.* (*BABAR* Collaboration), Phys. Rev. Lett.**97**, 171805 (2006); S.-W. Lin *et al.* (Belle Collaboration), Phys. Rev. Lett.**98**, 181804 (2007).
9. H.-Y. Cheng and K.-C. Yang, arXiv:0805.0329 [hep-ph] (2008).
10. B. Aubert *et al.* (*BABAR* Collaboration), Phys. Rev. Lett.**100**, 081801 (2008) ; B. Aubert *et al.* (*BABAR* Collaboration), arXiv:0806.4467 [hep-ex]
11. W. T. Ford, presented at FPCP, Taipei, 2008
12. *BABAR* Collaboration, B. Aubert *et al.*, Nucl. Instrum. Methods Phys. Res., Sect. **A479**, 1 (2002).
13. *BABAR* Collaboration, B. Aubert *et al.*, Phys. Rev. D **70**, 032006 (2004).
14. S. Agostinelli *et al.*, Nucl. Instrum. Methods Phys. Res., Sect. A **506**, 250 (2003).
15. A. Datta *et al.*, Phys. Rev. D. **77**, 114025 (2008).
16. ACCMOR Collaboration, C. Daum *et al.*, Nucl. Phys. B **187**, 1 (1981); E791 Collaboration, E. M. Aitala *et al.*, Phys. Rev. Lett. **86**, 765 (2001).
17. LASS Collaboration, D. Aston *et al.*, Nucl. Phys. B **296**, 493 (1988); *BABAR* Collaboration, B. Aubert *et al.*, Phys. Rev. D **72**, 072003 (2005).